J Mater Sci: Mater Electron (2016) 27:10798–10802
DOI 10.1007/s10854-016-5185-y

Electrospinning fabrication and luminescence of $La_3(BWO_9)$:Tb^{3+} nanofibers

Yanfeng Miao[1] · Peng Wang[2] · Huiyuan Guan[1] · Yulong Chen[1]

Received: 4 May 2016 / Accepted: 11 June 2016 / Published online: 16 June 2016

Abstract $La_3(BWO_9)$:Tb^{3+} nanofibers were fabricated by an electrospinning process. The XRD patterns of the obtained fibers indicate that the incorporation of Tb^{3+} ions will not change the phase of $La_3(BWO_9)$. The excitation spectrum monitored at 547 nm consists of excitation bands originating from $^1T_1 \rightarrow {}^1A_1$ transition of $O^{2-} \rightarrow W^{6+}$ in the WO_6 group and $^4f^8 \rightarrow {}^4f_7 5d^1/4f^8$ transitions of Tb^{3+}. Upon the excitation at 362 nm, $La_3(BWO_9)$:Tb^{3+} fibers show emission bands originating from the $^5D_4 \rightarrow {}^7F_j$ (j = 6, 5, 4 and 3) transitions of Tb^{3+}. The decay characteristics of La_3BWO_9:Tb^{3+}nanofibers indicate that Tb^{3+} ions occupy one site in the host lattice.

1 Introduction

The electricity consumption in domestic buildings occupies higher and higher percentage in whole electricity consumption. As a result, white light emitting diodes (WLEDs), having advantages of long lifetime, high luminescence efficiency, low power consumption and environment friendly characteristics, attract considerable research for solid-state lighting applications [1, 2]. In the fabrication of WLEDs, the combination of green and red emitting phosphors with a blue chip leads to the high color rendering and high efficiency [3]. Due to the intense and sharp luminescence originating from the f–f electronic transitions, rare earth ions are used widely as activators in phosphors. Among rare earth ions, Eu^{3+} [4–10] and Tb^{3+} [11–18] ions often act as activators to obtain red and green emissions. The green emission of Tb^{3+} mainly comes from the $^5D_4 \rightarrow {}^7F_j$ (j = 6, 5, 4 and 3) transitions.

Borate and tungstate phosphors for WLED applications have attracted much attention because of the broad and intense ligand-to-metal charge transfer band in the ultraviolet or near ultraviolet region, which is expected to capture the emission from a GaN-based LED in this range [10]. The mixed-anion rare earth compounds in combination with borate and tungstate have been reported in WO_3–Ln_2O_3–B_2O_3 system (Ln = rare earth ion), such as $Gd_4B_2WO_{12}$ [19], Eu_3BWO_9 [20] and $LaBWO_6$ [9]. In this work, we report on the luminescent properties of $La_3(BWO_9)$:Tb^{3+} nanofibers fabricated by an electrospinning method. Nanofiber-phosphors have obvious advances owing to their anisotropy, large width-thickness ratio and length-diameter ratio, unique optical, electrical and magnetic properties [21]. Electrospinning technology has been extensively explored as a simple and versatile method for forming inorganic superfine nanofibers using polymer/inorganic composite as the precursor. The morphology of fine products fabricated by electrospinning can be controlled by adjusting experimental parameters, such as the precursor solution viscosity, the structure of spinneret, voltage and the distance between the spinneret and the collector.

2 Materials and methods

A series of $La_3(BWO_9)$:x mol%Tb^{3+} (x = 2, 3, 4, 5 and 6) nanofibers were fabricated by an electrospinning process. La_2O_3 (99.99 %), Tb_4O_7 (99.99 %), H_3BO_3 (99.99 %), $(NH_4)_{10}H_2(W_2O_7)_6$ (99.95 %) were used as raw materials.

✉ Huiyuan Guan
hyguannj@sina.com

[1] College of Furniture and Industrial Design, Nanjing Forestry University, Nanjing 201137, China

[2] School of Materials and Engineering, Shandong University, Jinan 250061, China

Citric acid (99.5 %) and polyvinyl pyrrolidone (PVP, $M_w = 90{,}000$) were used as additives. All chemicals were used directly without further purification.

Spinning solution was prepared firstly for fabrication of $La_3(BWO_9):Tb^{3+}$ nanofibers. In a typical preparation, 1.3 mmol of La_2O_3 and 0.1 mmol of Tb_4O_7 were dissolved into 10 mL of hot aqueous nitric acid solution to form the solution A. Then, 1 mmol of H_3BO_3 and 0.083 mmol of $(NH_4)_{10}H_2(W_2O_7)_6$ were dissolved into 10 mL of deionized water containing citric acid to form the solution B. The molar ratio of La + Tb to citric acid was kept at 1:2. Precursor solution was obtained by mixing solutions A and B under continuous stirring. Finally, 3.0 g of PVP was added to the precursor solution and mixed to form a homogeneous spinning solution. During the process of electrospinning, the spinning solution was loaded into a plastic syringe with a spinneret, and the angle between spinneret and horizon was fixed to 10° for fabricating nanofibers. A flat iron net was used as the collector putting about 18 cm away from the spinneret. The flow rate was kept at 0.5 mL/h. The voltage of direct current adjusted to 15 kV was applied between the spinneret and the collector to generate the stable continuous PVP-based composite nanofibers. The obtained fibers were dried in an oven at 120 °C for 2 h and then heated at 800 °C for 5 h.

The X-ray powder diffraction (XRD) measurements were carried out on a Rigaku-Dmax 2500 diffractometer using Cu Kα radiation ($\lambda = 0.15405$ nm). The morphology and structure of the samples were inspected by an FESEM-4800 field emission scanning electron microscope (SEM, Hitachi). The luminescence was performed on a HitachiF-7000 spectrophotometer equipped with a 150 W xenon lamp as the excitation source. The decay curves were obtained from a Lecroy Wave Runner 6100 digital oscilloscope (1 GHz) using a tunable laser (pulse width = 4 ns, gate = 50 ns) as excitation source (Continuum Suncite OPO).

3 Results and discussion

The phase of $La_3(BWO_9):xmol\%Tb^{3+}$ (x = 2, 3, 4, 5 and 6) after the heating at 800 °C are confirmed by XRD patterns. $La_3(BWO_9)$ crystallizes in a hexagonal structure with the $P6_3$ space group. W atoms in the structure are surrounded by six oxygen atoms, forming a trigonal-prismatic coordination, which shares edges with three rare-earth polyhedrons. La atoms adopt ninefold coordination, of which six O atoms are derived from three WO_6 groups by sharing one edge with a WO_6 trigonal prism and the other three O atoms from BO_3 groups. LaO_9 polyhedrons connect each other by sharing the corner O atoms of WO_6 and BO_3 groups, forming the framework of La_3BWO_9. As shown in Fig. 1, the XRD patterns of all samples are identical and match well with that of the pure La_3BWO_9 with a hexagonal structure (JCPDS No. 77-1040). No other impurity peaks can be detected. These results suggest that Tb^{3+} ions have doped into the La_3BWO_9 host lattice entirely and form the complete solid solution. Due to the same valence state and similar ionic radii, Tb^{3+} ions will substitute La^{3+} ions in La_3BWO_9. The diffraction peaks of these samples are broadened remarkably, which reveals their nanocrystalline structure. The average crystallite sizes of samples can be calculated by the Scherrer equation:

$$D = \frac{K\lambda}{\cos\theta\sqrt{\beta^2 - \beta_0^2}} \quad (1)$$

where D is the average grain size, K = 0.9 is a characteristic for spherical objects, λ is the X-ray wavelength, θ and β are the diffraction angel and full-width at half-maximum of an observed peak. On the basis of diffraction peak of (201), the average grain sizes are calculated to be about 20 nm.

To show the morphology and size of the samples, the SEM images are obtained. Figure 2 shows the SEM images of $La_3(BWO_9)$:5 mol%Tb^{3+} after the heating at 800 °C. As shown in Fig. 2a, a large number of uniform fibers with diameters about 150 nm are obtained. The enlarged SEM image (Fig. 2b) shows that these fibers are rough and comprised of nanoparticles with sizes about 20 nm. The rough surface is induced by the removal of the residual organic solvent and PVP, plus the agglomeration of nanoparticles to form nanofibers during the electrospinning and heating processes. All samples have the same morphology and size. The morphology and diameter of the

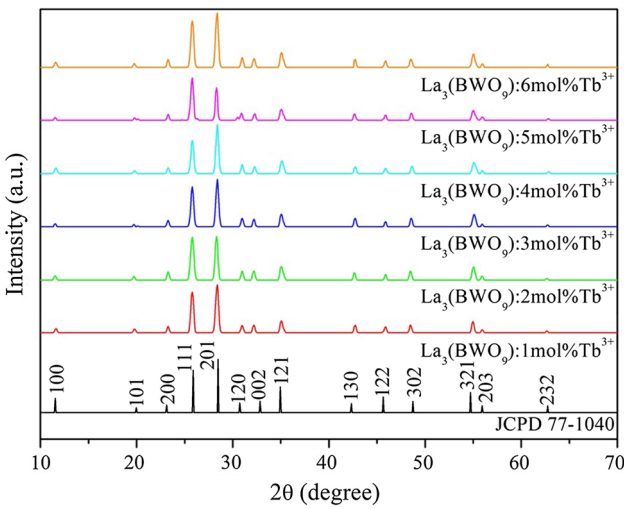

Fig. 1 XRD patterns of $La_3(BWO_9):Tb^{3+}$ nanofibers and standard XRD data of $La_3(BWO_9)$

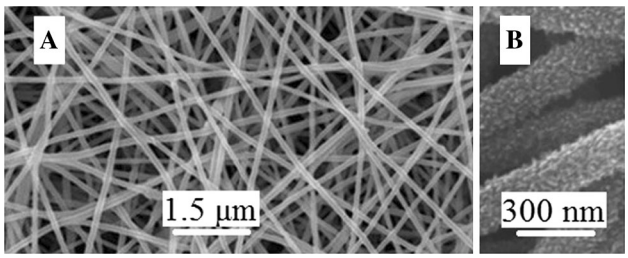

Fig. 2 SEM images of $La_3(BWO_9)$:5 mol%Tb^{3+} nanofibers

electrospun samples depend on the intrinsic properties of the solution and the operational conditions. In order to obtain fibers with perfect uniform morphology, the key is searching a balance point of various electrospinning parameters, such as the volume ratio of deionized water to citric acid, the weight percentage of PVP, the spinning rate, the strength of the electric field, and the distance between the spinneret and the collector.

Figure 3 shows the excitation and emission spectra of $La_3(BWO_9)$:5 mol%Tb^{3+} nanofibers. The excitation spectrum consists of two parts by monitoring the emission at 547 nm. The broad band maximized at 296 nm is ascribed to charge transfer from the ligand to the metal, derived from the $^1T_1 \rightarrow {}^1A_1$ transition of $O^{2-} \rightarrow W^{6+}$ in the WO_6 group [10] and the $^4f^8 \rightarrow {}^4f_7 5d^1$ transition of Tb^{3+} ions [22]. Those excitation bands in the range of 300-400 nm come from the $4f^8 \rightarrow 4f^8$ transitions from the ground $^7F_6$ level to excited $^{2S+1}L_J$ of Tb^{3+} ions [23]. There is a weakness of the interconfigurational $^4f^8 \rightarrow {}^4f^7 5d^1$ transition comparing to the $4f^8 \rightarrow 4f^8$ transitions although the former is parity allowed and thus usually much stronger, because that the $^4f^n \rightarrow {}^4f^{n-1}5d^1$ transitions within the conduction band will lose the superior intensity as has been shown for the Ce^{3+}-doped $Y_3Al_5O_{12}$ single crystals [24]. Upon the excitation at 362 nm, four typical emission peaks at 489, 547, 589 and 623 nm originating from $^5D_4 \rightarrow {}^7F_j$ (j = 6, 5, 4 and 3) transitions of Tb^{3+} ions can be observed. Among them, the green emission band at 547 nm originating from the $^5D_4 \rightarrow {}^7F_5$ transition is strongest.

The dependence of emission intensity on Tb^{3+} doping concentration is shown in Fig. 4. Upon the excitation of 362 nm, $La_3(BWO_9)$:xmol%Tb^{3+} (x = 2, 3, 4, 5 and 6) nanofibers show emission bands originating from $^5D_4 \rightarrow {}^7F_j$ (j = 6, 5, 4 and 3) transitions of Tb^{3+} ions and the increasing concentrations of Tb^{3+} ions bring no obvious alteration in the shapes of emission spectra. The almost complete absence of emission bands originating from $^5D_3 \rightarrow {}^7F_j$ transitions means that the emission from the $^5D_3$ level is quenched and the excitation energy ends to the $^5D_4$ level instead. The weakness of the $^4f^8 \rightarrow {}^4f^7 5d^1$ transitions in the excitation spectrum offers a plausible explanation for the absence of $^5D_3$ emission: the $^5D_3$ level locates in the conduction band of La_3BWO_9, and the $^5D_3$ emissions are quenched to the lowest emitting level, $^5D_4$, via the conduction band. The emission intensity increases with the increasing concentrations of Tb^{3+} and reaches the maxima for $La_3(BWO_9)$:5 mol%Tb^{3+}, then decreases with the further increase of Tb^{3+} concentration. The increases of emission intensity with the increasing concentrations of Tb^{3+} is attributed to a large number of luminescent centers up to a critical concentration, beyond which a decrease in the emission intensity occurs due to the concentration quenching effect. Quenching can originate from efficient energy transfer among the dopant ions, because of the matching of their energy levels, followed by the eventual energy transfer from the dopant ions to a defect where nonradioactive decay occurs. The occurrence of nonradiative

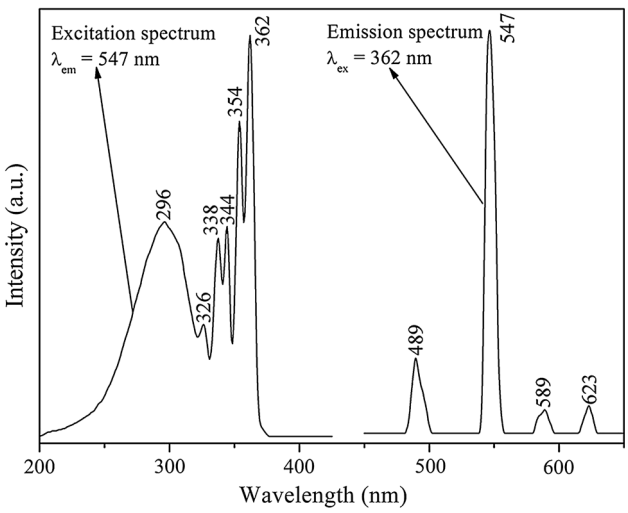

Fig. 3 Excitation and emission spectra of $La_3(BWO_9)$:5 mol%Tb^{3+} nanofibers

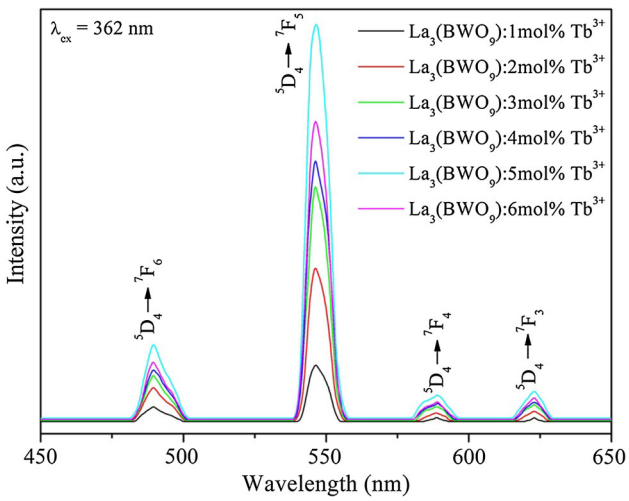

Fig. 4 Emission spectra of $La_3(BWO_9)$:Tb^{3+} nanofibers

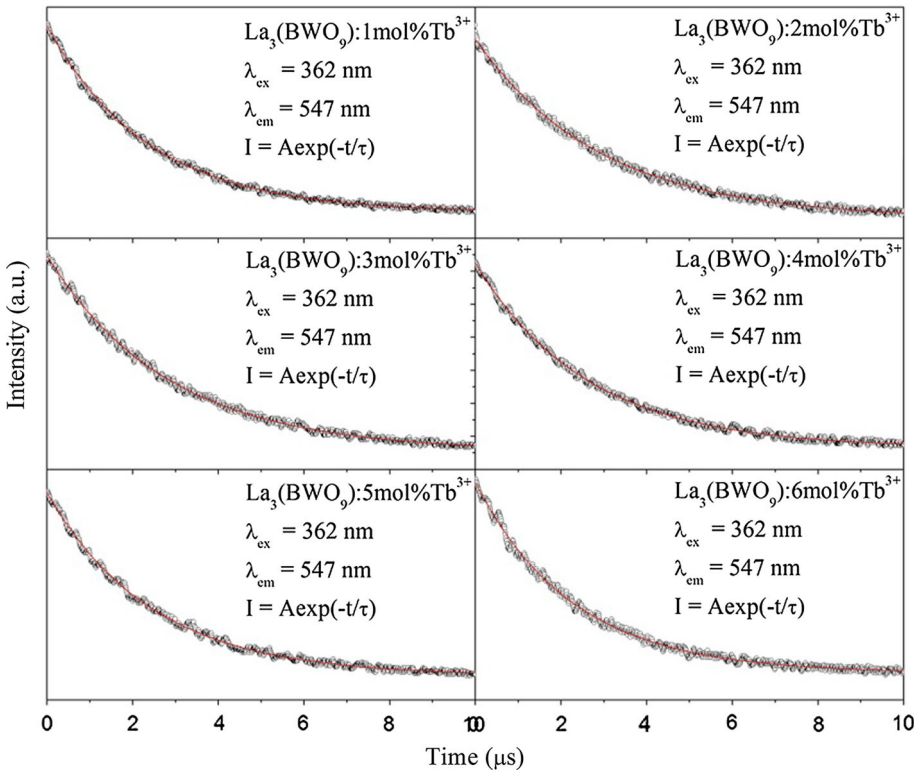

Fig. 5 Decay curves of $La_3(BWO_9):Tb^{3+}$ nanofibers

energy transfer may be caused by exchange interaction, radiation reabsorption, or multipole–multipole interaction [25]. The exchange interaction is a short-distance interaction and the typical critical distance is about 5 Å. The critical transfer distance (R_c) can be calculated by the formula of

$$R_C \approx 2(3V/4\pi XN)^{\frac{1}{3}} \quad (2)$$

where X is the critical concentration of Tb^{3+}, V is the volume of the unit cell, and N is the number of available sites of the dopant in the unit cell. For $La_3BWO_9:Tb^{3+}$nanofibers, V = 371.05 Å, X = 0.05 and N = 6, the critical transfer distance of Tb^{3+} in La_3BWO_9 is calculated to be 13.32 Å. And the mechanism of radiation reabsorption comes into effect only when there is a broad overlap of the emission spectrum of the sensitizer and the excitation spectrum of the activator. Since the critical transfer distance is larger than 5 Å and there is no overlap between the excitation and emission spectra of $La_3BWO_9:Tb^{3+}$, the energy transfer process should be controlled by the multipole–multipole interaction.

To obtain additional information on the luminescent properties of the Tb^{3+} ions in $La_3(BWO_9)$ host, the decay curves of the Tb^{3+} emission at 547 nm corresponding to the $^5D_4 \rightarrow {}^7F_5$ transition upon 362 nm excitation for $La_3(BWO_9)$:xmol%Tb^{3+} nanofibers are measured, as shown in Fig. 5. All of curves demonstrate almost perfect single-exponential function:

$$I = A\exp(-t/\tau) \quad (3)$$

where I is the emission intensity at time of t, A is a constant, t is the time, τ is the decay time. This suggests that Tb^{3+} ions occupy one site in the host lattice. The decay times for $La_3(BWO_9)$:xmol%Tb^{3+} (x = 2, 3, 4, 5 and 6) are 2.896, 2.821, 2.608, 2.448, 2.365 and 2.290 ms, respectively.

4 Conclusion

$La_3BWO_9:Tb^{3+}$nanofibers have been fabricated via an electrospinning process. The phase structure, size and morphology and luminescent properties have been studied as a function of Tb^{3+} concentration. The results suggest that the Tb^{3+} concentration in La_3BWO_9 host will not change the phase structure and morphology of $La_3BWO_9:Tb^{3+}$nanofibers, but has obvious influence on the luminescent properties. The emission intensity increases with the increasing concentrations of Tb^{3+} and reaches the maximum for $La_3(BWO_9)$:5 mol%Tb^{3+}, then decreases with the further increase of Tb^{3+} concentration because of the concentration quenching effect. The decay characteristics of $La_3BWO_9:Tb^{3+}$nanofibers indicate that Tb^{3+} ions occupy one site in the host lattice.

Acknowledgments The work is supported by the Priority Academic Program Development of Jiangsu Higher Education Institutions (PAPD).

References

1. S. Tonzani, Nature **459**, 312 (2009)
2. S. Pimputkar, J.S. Speck, S.P. Denbaars, S. Nakamura, Nat. Photonics **3**, 180 (2009)
3. P. Falcaro, S. Furukawa, Angew. Chem. Int. Ed. **51**, 8431 (2012)
4. Z. Zhang, L. Liu, S. Song, J. Zhang, D. Wang, Curr. Appl. Phys. **15**, 248 (2015)
5. X. Lu, J. Mater. Sci. Mater. Electron. **25**, 952 (2014)
6. Y. Yang, X. Wang, B. Liu, Nano **9**, 1450008 (2014)
7. G. Chen, F. Wang, W. Ji, Y. Liu, X. Zhang, Superlattices Microstruct. **90**, 30 (2016)
8. Y. Yang, Mater. Sci. Eng. B **178**, 807 (2013)
9. Z. Liu, X. Wang, W. Xu, Z. Xia, Superlattices Microstruct. **89**, 259 (2016)
10. J. Huang, B. Hou, H. Ling, J. Liu, X. Yu, Inorg. Chem. **53**, 9541 (2014)
11. Y. Liu, X. Yue, K. Cai, H. Deng, M. Zhang, Energy **93**, 1412 (2015)
12. B. Li, H. Zhang, A. Lan, H. Tang, Chem. Phys. Lett. **636**, 22 (2015)
13. T. Grzyb, M. Runowski, A. Szczeszak, S. Lis, J. Phys. Chem. **116**, 17188 (2012)
14. Y. Tian, Y. Fang, B. Tian, C. Cui, P. Huang, L. Wang, H. Jia, B. Chen, J. Mater. Sci. **50**, 6060 (2015)
15. X. Zhang, X. Zhang, Z. Zhao, J. Chaudhuri, J. Mater. Sci. **50**, 251 (2015)
16. F.-C. Lu, L.-J. Bai, T. Lu, W. Dang, Z.-P. Yang, P. Li, J. Am. Ceram. Soc. **98**, 867 (2015)
17. M. Srinivas, B. Appa Rao, M. Vithal, P. Raghava Rao, Luminescence **28**, 597 (2013)
18. Y. Zhang, V. Vijayaragavan, G.K. Das, K. Bhakoo, T.T.Y. Tan, Eur. J. Inorg. Chem. **12**, 2044 (2012)
19. R. Zhu, Y. Huang, H.J. Seo, J. Am. Ceram. Soc. **94**, 3380 (2011)
20. R. Zhu, Y. Huang, H.J. Seo, J. Electrochem. Soc. **157**, H1116 (2010)
21. W. Ma, W. Yu, X. Dong, J. Wang, G. Liu, Chem. Eng. J. **244**, 531 (2014)
22. C. Qin, L. Qin, G. Chen, T. Lin, Mater. Lett. **106**, 436 (2013)
23. L.C.V. Rodrigues, H.F. Brito, J. Hölsä, R. Stefani, M.C.F.C. Felinto, M. Lastusaari, T. Laamanen, L.A.O. Nunes, J. Phys. Chem. C **116**, 11232 (2012)
24. T. Tomiki, H. Akamine, M. Gushiken, Y. Kinjoh, M. Miyazato, T. Miyazato, N. Toyokawa, M. Hiraoka, N. Hirata, Y. Ganaha, T. Futemma, J. Phys. Soc. Jpn. **60**, 2437 (1991)
25. L.G. Van Uitert, J. Electrochem. Soc. **114**, 1048 (1967)